

**A MOBILE ROBOTIC PLATFORM FOR AUTONOMOUS NAVIGATION AND DEXTEROUS
MANIPULATION IN AN UNSTRUCTURED ENVIRONMENT**

Paul M. MOUBARAK

Robotics and Mechatronics Lab
Mechanical And Aerospace Engineering
The George Washington University
Washington, DC, USA

Pinhas BEN-TZVI

Robotics and Mechatronics Lab
Mechanical And Aerospace Engineering
The George Washington University
Washington, DC, USA
bentzvi@gwu.edu

Zhou MA

Robotics and Mechatronics Lab
Mechanical And Aerospace Engineering
The George Washington University
Washington, DC, USA

Kirk M. SUTHERLAND

Robotics and Mechatronics Lab
Mechanical And Aerospace Engineering
The George Washington University
Washington, DC, USA

Melanie DUMAS

Defense Advanced Research Projects Agency
Information Processing Techniques Office
3701 Fairfax Drive, Arlington, VA 22203-1714

ABSTRACT: A key element for advances in robotics research is the availability of a robotic platform that serves as a test-bench to evaluate the practicality of simulation results and the feasibility of novel theoretical findings. This paper presents the design and analysis of an intelligent robotic platform we developed as an experimental set-up for our subsequent and on-going work on mobile robot autonomy. The presented Hybrid Mobile Mechanism Robot (HMMR) combines locomotion with manipulation in a symmetric mobile platform. The HMMR is also equipped with measurement and sensing tools, such as LIDAR and stereo vision, as well as a single board computer for data processing and synthesis of actions. We present hardware details, discuss sensor layouts and wireless data communication between different links of the robot, and examine the capabilities of the manipulator's end-effector. Ultimately, our objective is to use the established platform to develop and test algorithms that automate the HMMR's ability to negotiate obstacles and maneuver objects in space.

Keywords: Mobile Robots, Autonomous, Navigation, Manipulation

I- INTRODUCTION

Traditionally, locomotion for robotic platforms has been implemented using conventional mobility techniques, such as

wheels [1] and tracks [2, 3]. These mechanisms are normally well suited for locomotion on unobstructed terrains; however their ability to overcome obstacles is often limited by their geometry. To address this problem and enable mobile platforms to overcome obstacles, alternative mobility techniques have been developed and reported. These include legged robots [4, 5], mobile structures with hopping [6, 7] and undulating capabilities [8, 9], or other variations of the wheeled [10] and tracked platforms [11, 12] and structures that combine two or more locomotion modes [13, 14].

Yet, enabling mobile robotic platforms to overcome obstacles by introducing non-traditional mobility techniques has often been developed at the expense of other important features of robotic applications, such as manipulation and dexterous interaction with the surroundings. In the past, we addressed this problem by developing a symmetric robotic platform (HMR) [15]–[17], [22, 23] that maintains mobility under flip-over conditions and enables the robot to overcome obstacles by using its manipulator arm as leverage. Furthermore, the manipulator arm (of the HMR) carried a gripper at the end-link level which provided object handling and maneuvering capabilities. In the current work, we focus on autonomy where we aim at automating the process of avoiding obstacles and manipulating objects using a modified version of the HMR. These autonomous capabilities are desirable for robotic applications that require a high-level of operation

independence, such as during search and rescue missions or military reconnaissance operations.

The literature reports an ample amount of work on robotic autonomous obstacle avoidance and manipulation. Techniques such as using visual perception to navigate in indoor environment, locate and manipulate objects have been reported for house-hold robots [18] or personal robots with dual-arm platforms [19]. Other techniques, such as building 3-D maps of the surroundings and searching for objects in a household environment have been accomplished on mobile robots [20] with the WAM arm [21] and a SEGWAY platform.

The work reported in [18] is a close general illustration of our ongoing and prospective research endeavors. However, our efforts are tailored towards outdoor applications requiring mobile robots to perform autonomous manipulation and obstacle avoidance maneuvers. To achieve this, we developed a tracked robotic platform (HMMR) with a symmetric morphology that carries a central manipulator arm with a dexterous end-effector. The platform is equipped with vision and scanning sensors for environment mapping and object recognition, inertial measurement units for navigation and position sensors for robust manipulation. Our objective is to use this platform to tackle the challenges associated with autonomous obstacle avoidance and manipulation of mobile robots operating in and around unstructured environments, such as stairs, or uneven terrain topologies in war-zones and collapsed buildings in the aftermath of earthquakes.

II- OVERALL STRUCTURAL DETAILS OF THE HMMR

The overall structural layout of the robot presented in this paper is shown in Figure 1, in the folded and closed configuration, and in Figure 2, in the unfolded and opened configuration. The capabilities of a Hybrid Mobile Robot (HMR) have been demonstrated in [15] – [17]. In this effort, we extrapolate on our previous work and design a smaller, compact and more efficient generation of hybrid mechanism mobile robots (HMMR) with overall dimensions of 530(W)×630(L)×140(H) mm and a calculated weight of 45Kg. The HMMR accommodates a larger and more dexterous end-effector, as well as a variety of sensors and mechanisms that pertain directly to our subsequent work in robotic autonomy.

Overall, the HMMR incorporates two tracked platforms actuated independently and providing traction to the robot. A central manipulator arm with two links and two degrees of freedom (DOF) is cascaded between the tracks. The actuation of these DOF's is performed separately via motors located under the tracks. For convenience, in the remainder of the paper, we will refer to the tracked platform as Link 1 (Left and Right with respect to the manipulator arm when facing the end-effector), the middle link of the manipulator arm as Link 2, and the top link as Link 3.

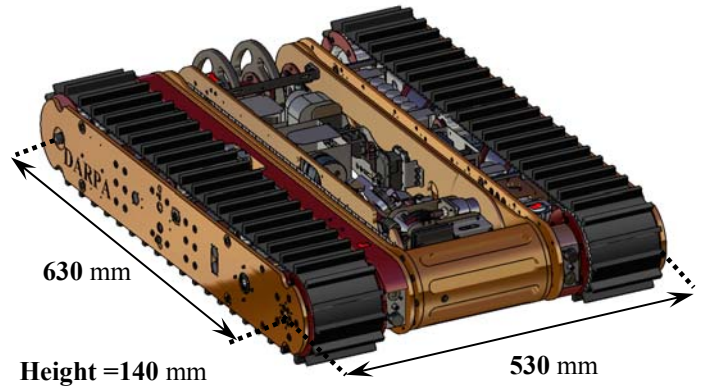


Figure 1: Overall layout of the HMMR in the folded configuration

An end-effector is carried by the manipulator arm as shown in Figure 2. This end-effector is a self-contained entity of the HMMR, comprising three fingers and providing three separate DOF's. In addition to the robotic hand, Link 3 accommodates a servo-actuated mechanism that carries a 2-D LIDAR and a stereo camera. A single board computer is also housed inside the link. This connects directly to the camera and LIDAR in order to process images and synthesize actions accordingly. Many additional components, such as proximity sensors, inertial measurement units, encoders, GPS and RF transmitters and receivers are spread all across the robot. Details of these will be further discussed in the subsequent sections.

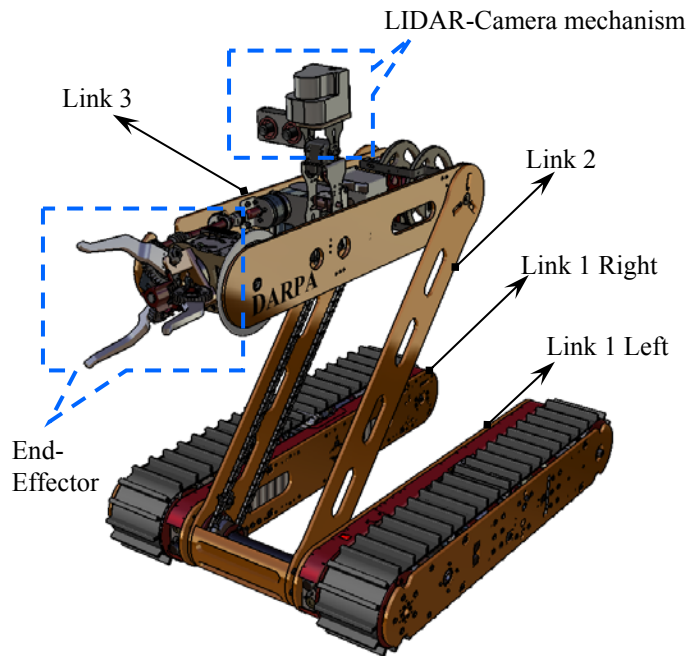


Figure 2: Overall layout of the HMMR in the unfolded and opened configuration

III- MECHANICAL AND ELECTRICAL LAYOUT

Mechanically, the HMMR is driven by two sets of tracked platforms. Each platform is actuated by a brushless DC motor generating 212 Watts of power and operating at 45Volts. A peak torque of 21[N·m] at 96[RPM] is available at the active pulleys of each track (Figure 3.a). To generate this torque from an initial motor output of 0.22[N·m], two amplification stages were implemented. First, a planetary gearhead couples directly to the motor output shaft and provides a reduction ratio of 1:32. A second amplification stage is implemented using bevel gears. This couples to the planetary gearhead and provides an additional amplification factor of 1:3. The resulting amplification ratio of 1:96 provides enough torque to allow the robot to climb steep terrains of up to 60° in inclination, making it ideal for applications requiring stairs climbing.

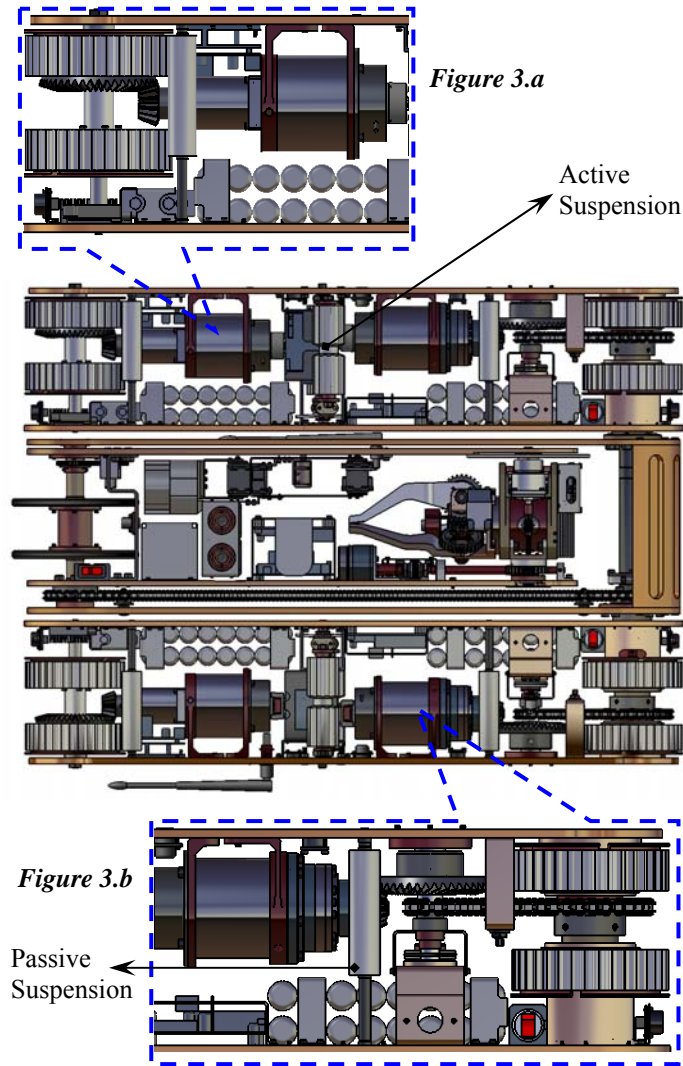


Figure 3: Top view of the HMMR without tracks, showing close-up views of the two motor assemblies under the tracks; a) Active pulley assembly b) Passive pulley assembly

On the other hand, in order to optimize the dimensions and place the motors under the tracks, the active pulleys were modified in a way to align the motor-gearhead shaft with the central plane of the pulleys (Figure 3.a). This allowed us to integrate the larger bevel gear within the structure of the pulley and thereby reduce the space needed to implement this mechanism. The motor assembly also includes a spring applied brake coupled directly to the back shaft of the motor and providing a static braking torque of 0.79N.m.

Similar motor assemblies were adopted to actuate the two DOF's of the manipulator arm. Both DOF's were driven via sprocket-chain mechanisms by motors placed under the tracks of Link 1. However in this case, instead of using planetary gearheads, we used harmonic drives with a 1:120 amplification ratio. Two additional amplification stages were implemented in order to generate a desired output torque of 150N.m and a desired angular velocity of 50°/sec. These include a spiral bevel gear assembly with an amplification ratio of 1:3, and another sprocket-chain assembly providing an additional amplification of 1:2.9 (Figure 3.b). It is noteworthy to mention here the symmetry in the hardware layout between Link 1 Left and Link 1 Right.

Since both motors were placed under the tracks, the passive pulleys located at the other end of Link 1 had to be split in two sections. This allowed us to accommodate the sprocket-chain amplification stage between the passive pulley assembly (Figure 3.b). Direct coupling to the sprocket-driven shaft in Link 1 Left provides actuation to Link 2, while Link 3 necessitates an additional sprocket-chain mechanism with a 1:1 ratio and a chain running along Link 2, in order to transmit the torque from Link 1 Right to the axis of rotation of Link 3. Support to the manipulator arm was accomplished using a set of passive wheels, one located at the bottom of Link 3, the other at the tip. These wheels were not actuated, rather were allowed to roll freely whenever in contact with the ground.

We also note the use of a conjunction of active and passive suspensions to concurrently support and tension the tracks. Support and frame alignment was provided by four passive rollers, two on each side of Link 1 (Left and Right), while tensioning and shock absorption was provided by two central spring-actuated suspensions. These suspensions were implemented using torsional springs, and provide torsional damping for up to 25° in angular deflection under applied loading.

Electrically, the four motors located under the tracks are controlled using four quadrant motor controllers (DZRALTE-020L080) customized to accommodate the compact size of the robot and other control functions. These controllers provide position and speed control at a maximum continuous current output of 12Amps. Absolute encoders were also incorporated in the layout to keep track of all DOF's of the manipulator arm. These include a 12-bit magnetic encoder to monitor the angular rotation of Link 2, as well as a similar encoder to monitor the rotation of Link 3. Additional encoders were implemented

within the structure of the end-effector mechanism and will be discussed in more details in section V.

For navigation and path planning applications, a 20-channel compact GPS unit (MN5010HS) was mounted at the back of Link 1. Position error of the selected GPS is less than 3 meters, with a power consumption of less than 100mW. In conjunction with the GPS unit, an MTi inertial measurement unit (IMU) was also configured on Link 1 to provide information on acceleration, roll, pitch and yaw angles over the full range of 360° at an updating rate of 512Hz. We also note the use of sonar sensors with an active sensing range of 3 – 600 cm; one in the front, one in the back and two on the side of each module of Link 1 (Left and Right). As such, the GPS, the IMU and the sonars, in addition to the LIDAR and the stereo camera mounted on Link 3 (which will be discussed later in section IV), will provide significant dynamic information for our subsequent work on path planning, navigation and obstacle traversal and avoidance algorithms.

The main brain of the robot is housed in Link 3. This takes the form of an Intel® Atom based single board computer (SBC) that meets the PC/104-Plus form factor. The SBC has a 1.6GHz processor, along with 2GB of DDR2-400/533 DRAM and 4GB on a solid state drive. For the operating system, Ubuntu 9.10 (Karmic Koala) is installed. This OS has POSIX message queues available that allow for quick and easy inter-process communication. The SBC, not only connects to the LIDAR and the stereo cameras for image processing applications, but also receives data from the encoders and all other measurement units (GPS, IMU, sonars) over a wireless network to subsequently process and execute autonomous functionalities.

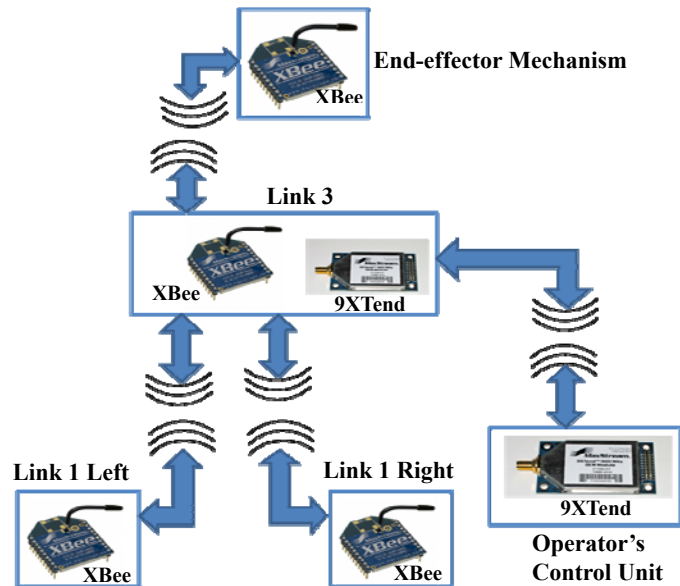


Figure 4: The RS485 network established between different links of the HMMR and with the operating unit (OCU)

On the other hand, the HMMR also incorporates a wireless implementation of an RS485 network as shown in Figure 4. Digi international's XBee 802.15.4 OEM RF modules are used with RS485 transceiver ICs to create a 2.4 GHz network over which data is shared between the links and with the operator. For this purpose, ARM7 processors that act as local controllers for non-RS485 devices are implemented on the PCB boards of each link. For longer range communications, such as between the robot and a remote operating unit (OCU), a 1Watt 9XTend module is used, capable of transmitting data at 900MHz for up to 20Km via a servo-actuated dipole antenna that rotates from side to side when the robot is flipped.

Finally, the robot is powered by different lithium-ion battery units. Link 1 Left and Link 1 Right each accommodates a 44.4Volts battery assembly with a capacity of 7.8Ah, capable of delivering 15Amps of continuous current discharge. Conversely, Link 3 operates under 15Volts provided by another battery assembly with a total capacity of 5.2Ah and a maximum continuous current discharge of 10Amps.

IV- NAVIGATIONAL SYSTEM

The main navigational and perception system on-board the HMMR is comprised of a servo-actuated LIDAR and stereo camera mechanism shown in Figure 5. The customized configuration of the two CCD cameras with a baseline of 41.5mm provides depth information on the environment. This information, sampled at a rate of 5 frames per second, is used to build a local map of the robot's vicinity. To augment the visual perception of the robot, a 2-D LIDAR (UBG-04LX-F01) mounted on top of the stereo camera scans over 240° in the horizontal plane at an average scan time of 28msec/scan.

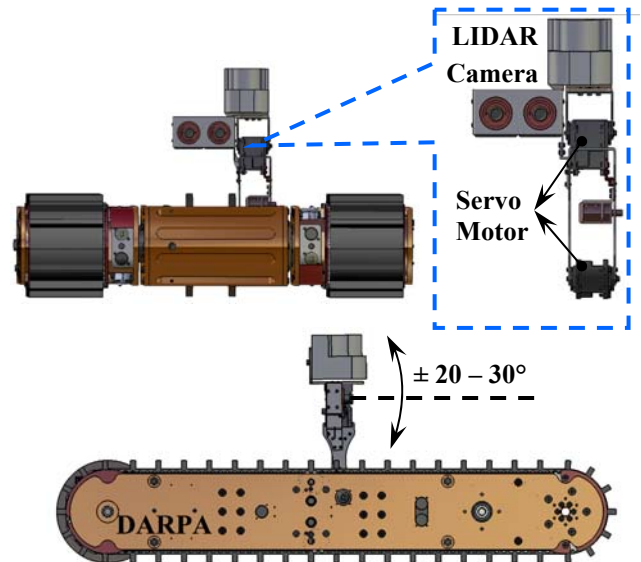


Figure 5: LIDAR-Stereo camera mechanism on-board the HMMR

Actuation of the LIDAR in the vertical plane enables the recognition of a 3-D environment, where the LIDAR scans the surroundings over a vertical range of $40 - 60^\circ$ ($\pm 20 - 30^\circ$ with respect to the horizontal plane). This actuation is accomplished by a 2-DOF mechanism operated by two servo motors, one located at the bottom which lifts the whole mechanism outside Link 3, the other, located under the LIDAR, enables the vertical scanning process. The latter is accomplished at an incremental pitch of 0.3° and is normally executed in 3.73 seconds. It is noteworthy to mention here that a 3-D visual perception of the environment is essential to our subsequent work on robotic autonomous navigation. Since the HMMR is a robot tailored to operate outdoors on unstructured terrains, the robot's ability to overcome obstacles using its manipulator arm cannot be exploited effectively in autonomous applications unless a 3-D representation of the environment is acquired.

A 3D visual perception of the environment is also essential for applications requiring autonomous manipulation. Object shape, object recognition via segmentation and depth information are gathered by processing images acquired by the stereo camera. However, more accurate information on the object dimensions as well as the object location with respect to the robot and the end-effector are acquired by processing LIDAR data.

Data from the LIDAR is also analyzed to acquire information on texture and detect edges in the surrounding environment. Surface detection enables autonomous climbing applications, by providing the robot with reference obstacle geometry and position to execute autonomous climbing maneuvers using its tracks and the manipulator arm. A sample scenario illustrating the described climbing maneuver will be later detailed in section VI. We recall here that data collected by the stereo camera and the LIDAR is processed on board the robot and synthesized into actions using the single board computer described in section III.

V- ROBOTIC END-EFFECTOR

As mentioned earlier in the context of the paper, the manipulator arm on-board the HMMR carries an end-effector that provides three fingers and three DOF's. The end-effector we describe in this section is a self-contained unit of the HMMR, in the sense that it carries its own batteries, motors, controllers, sensors, electronic boards and RF modules to communicate with the robot's main processing unit. This robotic hand, shown in Figure 6 in the exploded layout, is designed to handle a peak static load of 50Kg, weighs 2078grams and possesses the overall dimensions of 89(H) \times 124(W) \times 257(L) mm when fully assembled.

To operate the fingers (Angle Θ_1), a motor – gearhead assembly is housed inside the end-effector's wrist. This Maxon flat brushless DC motor (Diameter 45mm) provides 30 Watts of power for a rated speed of 4370 RPM when operating at a minimum voltage of 12Volts. A planetary gearhead couples

directly to the motor and provides a torque amplification ratio of 1:33. This in turn is further amplified by a worm and worm gear assembly providing an additional ratio of 1:15, and enabling a peak gripping force of 120N at the fingertips. The use of the worm and worm gear assembly is convenient in this case since it provides, in addition to torque amplification, braking means allowing us to eliminate the need and save the space occupied by a magnetic or a spring actuated brake. The motor controller (Θ_1) (EZSV23) located conveniently at the back of the motor, operates at 12 – 40Volts and provides up to 5Amps of continuous current. Angular position readings over the fingers' operating range of $0 - 110^\circ$ are provided by a compact rotary analog encoder adapted directly to one of the fingers. Readings from the encoder are transmitted to the end-effector's brain via wireless means enabling us to achieve practical endless rotation on the hand wrist and the fingers' platforms. Wireless communication is achieved via an RF module incorporated on the fingers' platform. We also note the existence of a wireless analog camera on the fingers' platform that relays live video feed of the maneuvering process to the operating unit. Power to the camera, the encoder and the RF module is provided by a 9Volts regular battery mounted directly on the finger's platform.

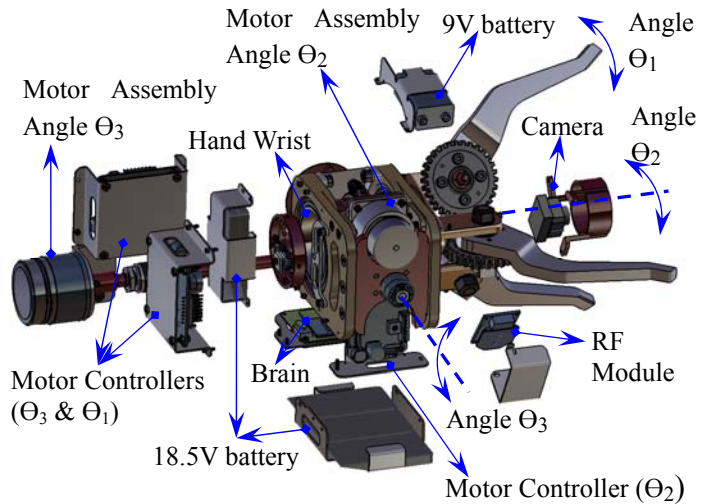


Figure 6: An exploded view of the end-effector mechanism in the opened configuration showing mechanical, electrical and structural details

A second motor assembly (Motor Assembly Angle Θ_2), provides rotation to the hand's wrist and the fingers' platform around the centroidal axis (Angle Θ_2). This rotation is practically endless and is achieved by a Maxon motor providing 15 Watts of power at a rated speed of 4460 RPM when operating at 12Volts. Two torque amplification stages, one implemented with a 1:30 spur gearhead, the other with a 1:30 worm gear assembly, provide a required torque of 12N.m for a rated angular velocity of the wrist of 30° /sec. Similar to angle Θ_1 , a motor controller (Θ_2) (EZSV17) is housed inside

the hand structure and provides 2Amps of continuous current. The angular position of the wrist is tracked by another encoder assembly coupled directly to the wrist for a 1:1 reading.

The third and final DOF is driven by a motor assembly (Motor assembly angle Θ_3) that rotates the whole hand assembly around the support shafts (Angle Θ_3). These shafts are resting on ball bearings housed inside the manipulator arm. In this case too, we used two torque amplification stages, one spur gearhead stage with a 1:47 ratio, the other, a worm gear assembly with a 1:15 ratio, together allowing us to generate a required torque of 21N.m at a rated angular velocity of 50°/sec. Encoders coupled directly to the support shafts provide angular position readings to the motor controller (EZSV23). All three motors, motor drivers, sensors and electronic boards are powered by a serial assembly of five Lithium-Ion cells, providing 18Volts with a peak continuous current discharge of 3.2Amps for a total capacity of 1.5Ah.

For convenience, we conclude this discussion with a summary of the end-effector specifications outlined in Table 1.

Table 1: Summary of the end-effector mechanism specifications for all three DOF's

Specification	Angle Θ_1	Angle Θ_2	Angle Θ_3
Motor Power	30 W	15 W	30 W
Motor Rated RPM	4370	4460	4370
Motor Operating Voltage Range	12 – 18 V	12 – 18 V	12 – 18 V
Number of Torque Amplification stages	2	2	2
Gearhead Ratio	1:33	1:30	1:47
Worm Assembly Ratio	1:15	1:30	1:15
Rated Final Output Torque	15.8 N.m	12 N.m	21 N.m
Rated Output Speed Range (under load)	50 – 75°/s	30– 45°/s	50– 75°/s
Operating Angular Range	0 – 110°	Endless	Endless
Motor Controller	EZSV23	EZSV17	EZSV23
Maximum Controller Current	5 A	2 A	5 A

To achieve ultimate compactness of the end-effector and to reduce the total weight of the assembly while optimizing the payload capability, a finite element model of the hand was developed and analyzed under different loading conditions. In

Figure 7, we show the propagation of stress from the fingers towards the support shafts for an applied load of 50Kg on a finger's tip.

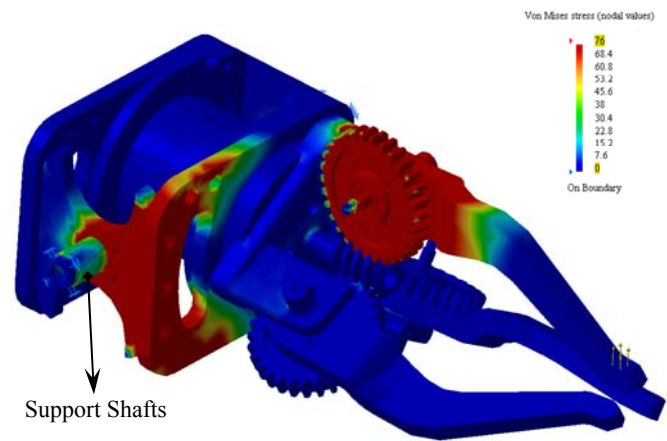


Figure 7: An FEA model of the end-effector showing stress propagation and stress concentration under fingers' loading

Because of the difficulty in predicting the propagation of stress from one part of the assembly to the other, an FEA analysis on an assembly model of the end-effector was favored over FEA analysis on individual parts. This approach yields the most accurate and realistic results and thereby allows us to optimize the weight and size of the hand and achieve high payload-to-weight ratios.

In the analysis shown in Figure 7, a clamp boundary condition was applied to the support shafts. All remaining parts of the assembly were constrained properly such that the whole assembly is fixed with respect to the clamps. We note here that parts that do not contribute directly to the structural analysis (such as motors, motor controllers, encoders...) and parts that we can model on the solver workbench, such as the tightening load of a screw or a nut, were ignored and not included in the analysis.

Using Von Mises criterion, we detected a peak stress of 76MPa at the loaded finger's worm gear. Because of the properties of the worm and worm gear mechanism that drives the fingers, the hand wrist did not experience significant axial loading, rather the loading remained in majority bending and was propagated away from the wrist towards the support shafts, hence shielding the shaft of the motor assembly of angle Θ_1 . We note here that although the actuators of the end-effector cannot alone maneuver a 50Kg load, the structure of the hand was proven strong enough to handle such load. Maneuvering in this case would be performed by the manipulator arm, with the end-effector providing static locking to all three DOF's by the worm and gear assemblies. Material selection and final dimensioning was ultimately performed based on these FEA results, where steel was chosen for critically stressed parts and aluminum for less stressed parts, thereby resulting in a total assembly weight of 2078grams as calculated by our CAD tools.

VI- CONCLUSION AND DISCUSSION OF FUTURE WORK

In this paper, we presented the design and analysis of the HMMR, a mobile robotic platform with a symmetric configuration and a manipulator arm. We discussed Mechanical and Electrical hardware layout, and detailed the on-board navigational system which is comprised of a servo-actuated mechanism that carries a LIDAR sensor and a stereo vision system. Putting the 2-D LIDAR on a pitch-actuated mechanism enables us to scan over the vertical plane and thereby extend the visual perception of the robot into the 3-D domain. We also presented a novel design for the robot's end-effector, which is a self-contained unit of the HMMR, and analyzed payload capabilities using an FEA assembly model of the end-effector mechanism.

Our subsequent work is tailored towards robotic autonomy, namely using the established platform to enable the development and the experimental validation of novel approaches for autonomous navigation and manipulation on unstructured terrains. In Figure 8, we illustrate a sample of the prospective research effort we will undertake with the HMMR.

The sample milestone includes the development of intelligent algorithms that enable the robot to overcome obstacles taller than its folded structure. These obstacles can represent furniture or stairs in a household indoor environment or rubble piles in the aftermath of an earthquake for outdoor search and rescue operations.

To achieve this, the HMMR will deploy its navigational system to scan the obstacle and gather information on its dimensions and position with respect to the robot's inertial frame, as well as to detect the outlining edges (Figure 8.a). An on-board algorithm will process this data and synthesize an appropriate action, which will dictate the subsequent configuration deemed most suitable to overcome the obstacle. This would often include using the manipulator arm to leverage the robot over the obstacle (Figure 8.b & 8.c) and reach the objective.

Likewise, descending an obstacle can be accomplished autonomously. In this case, the manipulator arm will be employed to augment the field of view of the navigational system and allow the robot to scan the underlying terrain using the LIDAR and the stereo camera (Figure 8.d). Images from both the LIDAR and the camera will be processed by an onboard algorithm and a subsequent descending configuration will be generated. This normally will include folding the LIDAR mechanism inside Link 3, and deploying the arm to roll on the ground to provide support and ultimately allow the robot to descend the obstacle (figure 8.e & 8.f).

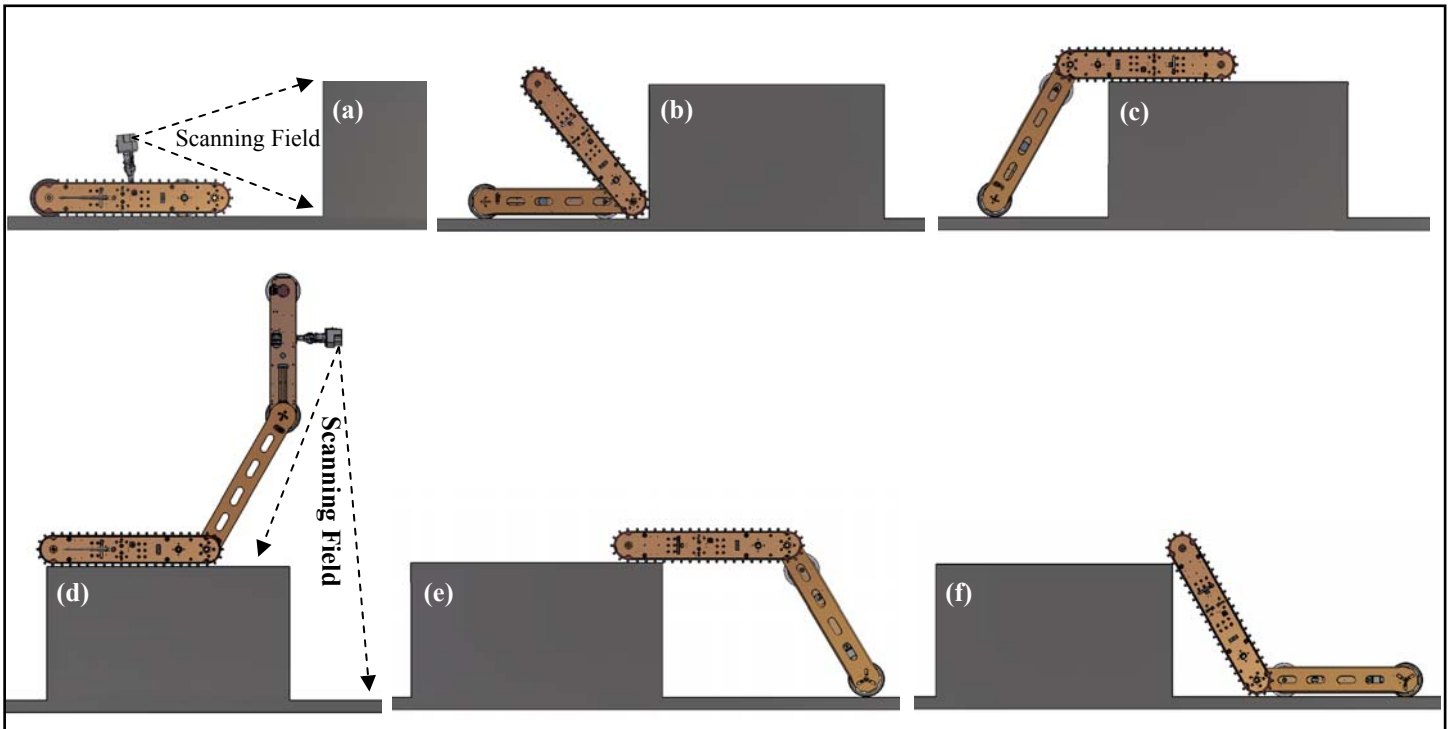


Figure 8: An illustration of a sample application of the HMMR showing the use of the navigational system and the manipulator arm to ascend and descend obstacles autonomously

ACKNOWLEDGEMENTS

This work is supported by the Defense Advanced Research Projects Agency (DARPA) under grant number R0011-09-1-0049. We also would like to acknowledge the support provided by the DARPA Program Manager, Ms. Melanie Dumas.

REFERENCES

- [1] LaoHu, Y., Tun, L., ZhiPing, Z., and WeiPing, Z., 2008, "Online Estimation of Wheel-ground Contact Angle and Slip for a Six-wheeled Lunar Rover", in *Proc. IEEE International Conference on Automation and Logistics, ICAL '08*, Qingdao, China, pp. 2059 – 2063.
- [2] Quan, Q., Ma, S., Li, B., and Liu, R., 2009, "Posture Control of a Dual-crawler-driven Robot", in *Proc. IEEE International Conference on Robotics and Automation, ICRA '09*, Kobe, Japan, pp. 2977 – 2982.
- [3] Liu, Y., and Liu, G., 2007, "Kinematics and Interaction Analysis for Tracked Mobile Manipulators", in *Proc. IEEE/RSJ International Conference on Intelligent Robots and Systems, IROS '07*, San Diego, CA, pp. 267 – 272.
- [4] Lida F, Rummel J, and Seyfarth A., 2008, "Bipedal Walking and Running with Spring-like Biarticular Muscles", *Journal of Biomechanics*, 41(3), pp. 656 – 667.
- [5] Chestnutt, J., Michel, P., Kuffner, J., and Kanade, T., 2007, "Locomotion Among Dynamic Obstacles for the Honda ASIMO", in *Proc. IEEE/RSJ International Conference on Intelligent Robots and Systems, IROS '07*, San Diego, CA, pp. 2572 – 2573.
- [6] Shin, Y., Kyoungu, R., Kim, T., Lee, J., Choi, J., Yim, C., and Kim, D., 2007, "Mechanism and Control of a Jumping Robot", in *Proc. IEEE/RSJ International Conference on Intelligent Robots and Systems, IROS '07*, San Diego, CA, pp. 2499 – 2502.
- [7] Niiyama, R., Nagakubo, A., and Kuniyoshi, Y., 2007, "Mowgli: A Bipedal Jumping and Landing Robot with an Artificial Musculoskeletal System", in *Proc. IEEE/RSJ International Conference on Intelligent Robots and Systems, IROS '07*, San Diego, CA, pp. 2546 – 2551.
- [8] Chen, L., Ma, S., Wang, Y., Li, B., and Duan, D., 2007, "Design and Modelling of a Snake Robot in Traveling Wave Locomotion", *Mechanism and Machine Theory*, 42(12), pp.1632 – 1642.
- [9] Bayraktaroglu, Z.Y., 2009, "Snake-like Locomotion: Experimentations with a Biologically Inspired Wheel-less Snake Robot", *Mechanism and Machine Theory*, 44(3), pp. 591 – 602.
- [10] Lindemann, R. A., and Voorhees, C. J., 2005, "Mars Exploration Rover Mobility Assembly Design, Test and Performance", in *Proc. 2005 IEEE International Conference on Systems, Man and Cybernetics*, Hawaii, USA, pp. 450 – 455.
- [11] Wang, W., Zhou L., Du, Z., and Sun, L., 2008, "Track-Terrain Interaction Analysis for Tracked Mobile Robot", in *Proc. IEEE/ASME International Conference on Advanced Intelligent Mechatronics, AIM '08*, Xi'an, China, pp. 126 – 131.
- [12] Masayuki, A., Takayama, T., and Hirose, S., 2004, "Development of "Souryu-III": Connected Crawler Vehicle for Inspection Inside Narrow and Winding Spaces", in *Proc. IEEE/RSJ International Conference on Intelligent Robots and Systems, IROS '04*, Sendai, Japan, pp. 52 – 57.
- [13] Michaud, F., Letourneau, D., Arsenault, M., Bergeron, Y., Cadrin, R., Gagnon, F., Legault, M-A., Millette, M., Pare, J-F., Tremblay, M-C., Lapage, P., Morin, Y., Bisson, J., Caron, S., 2003, "AZIMUT, a Leg-Track-Wheel Robot", in *Proc. IEEE/RSJ International Conference on Intelligent Robots and Systems, IROS '03*, Las Vegas, UT, pp. 2553 – 2558.
- [14] Wilcox, B. H., Litwin, T., Biesiadecki, J., Matthews, J., Heverly, M., Morrison, J., Townsend, J., Ahmad, N., Sirota, A., and Cooper, B., 2007, "ATHLETE: A Cargo Handling and Manipulation Robot for the Moon", *Journal of Field Robotics*, 24(5), pp. 421 – 434.
- [15] Ben-Tzvi, P., Goldenberg, A.A., and Zu, J.W., 2008, "Design and Analysis of a Hybrid Mobile Robot Mechanism with Compounded Locomotion and Manipulation Capability", *Journal of Mechanical Design*, 130, pp. 1– 13.
- [16] Ben-Tzvi, P., Goldenberg, A.A., and Zu, J.W., 2007, "Implementation of Sensors and Control Paradigm for a Hybrid Mobile Robot Manipulator for Search and Rescue Operations", In *Proc. IEEE International Workshop on Robotic and Sensors Environments (ROSE 2007)*, Ontario, Canada, pp. 92 – 97.
- [17] Ben-Tzvi, P., Goldenberg, A.A., and Zu, J.W., 2008, "Design, Simulations and Optimization of a Tracked Mobile Robot Manipulator with Hybrid Locomotion and Manipulation Capabilities", in *Proc. IEEE International Conference on Robotics and Automation, ICRA '08*, Pasadena, CA, pp. 2307 – 2312.
- [18] Stiickler, J., and Behnke, S., 2009, "Integrating Indoor Mobility, Object Manipulation, and Intuitive Interaction for Domestic Service Tasks", in *Proc. 9th IEEE-RAS International Conference on Humanoid Robots, Humanoids 2009*, Paris, France, pp. 506 – 513.
- [19] Rusu, R. B., Sucan, I. A., Gerkey, B., Chitta, S., Beetz, M., and Kavraki, L. E., 2009, "Real-time Perception-Guided Motion Planning for a Personal Robot", in *Proc. IEEE/RSJ International Conference on Intelligent Robots and Systems, IROS '09*, St. Louis, Missouri, pp. 4245 – 4252.
- [20] Srinivasa, S.S., Ferguson, D., Helfrich, C. J., Berenson, D., Collet, A., Diankov, R., Gallagher, G., Hollinger, G., Kuffner, J., VandeWeghe, M., 2010, "HERB: a home exploring robotic butler", *J. Auton. Robot*, 28, pp. 5 – 20.
- [21] The Barrett Hand™, Barrett Technology, <http://www.barrett.com/robot/products-hand.htm>, retrieved May 2010.
- [22] Ben-Tzvi, P., May 2010, "Experimental Validation and Field Performance Metrics of a Hybrid Mobile Robot Mechanism", *Journal of Field Robotics*, Vol. 27, Issue 3, pp. 250-267.
- [23] Ben-Tzvi, P., Goldenberg, A.A., Zu, J.W., "Articulated Hybrid Mobile Robot Mechanism with Compounded Mobility and Manipulation and On-Board Wireless Sensor/Actuator Control Interfaces", *Mechatronics Journal*, In Press, DOI 10.1016/j.mechatronics.2010.06.004.